AGU PUBLICATIONS

Geochemistry, Geophysics, Geosystems

RESEARCH ARTICLE
10.1002/2014GC005586

Key Points:
- Source of clay to Andaman Sea relatively constant for last 60 kyr
- Chemical weathering and South Asian monsoon stronger during the Holocene
- South Asian monsoon variability occurred on millennial timescales

Supporting Information:
- Supporting Information S1

Correspondence to:
S. Ali,
sa@gpi.uni-kiel.de

Citation:
Ali, S., E. C. Hathorne, M. Frank, D. Gebregiorgis, K. Stattegger, R. Stumpf, S. Kutterolf, J. E. Johnson, and L. Giosan (2015), South Asian monsoon history over the past 60 kyr recorded by radiogenic isotopes and clay mineral assemblages in the Andaman Sea, *Geochem. Geophys. Geosyst.*, *16*, 505–521, doi:10.1002/2014GC005586.

Received 2 OCT 2014
Accepted 21 JAN 2015
Accepted article online 28 JAN 2015
Published online 24 FEB 2015
Corrected 18 MAR 2015

This article was corrected on 18 MAR 2015. See the end of the full text for details.

South Asian monsoon history over the past 60 kyr recorded by radiogenic isotopes and clay mineral assemblages in the Andaman Sea

Sajid Ali[1,2], Ed C. Hathorne[1], Martin Frank[1], Daniel Gebregiorgis[1], Karl Stattegger[2], Roland Stumpf[3], Steffen Kutterolf[1], Joel E. Johnson[4], and Liviu Giosan[5]

[1]GEOMAR Helmholtz Centre for Ocean Research Kiel, Kiel, Germany, [2]Institute of Geosciences, Christian-Albrechts-University, Kiel, Germany, [3]Department of Earth Science and Engineering, Imperial College London, London, UK, [4]Department of Earth Sciences, University of New Hampshire, New Hampshire, Durham, USA, [5]Woods Hole Oceanographic Institute, Woods Hole, Massachusetts, USA

Abstract The Late Quaternary variability of the South Asian (or Indian) monsoon has been linked with glacial-interglacial and millennial scale climatic changes but past rainfall intensity in the river catchments draining into the Andaman Sea remains poorly constrained. Here we use radiogenic Sr, Nd, and Pb isotope compositions of the detrital clay-size fraction and clay mineral assemblages obtained from sediment core NGHP Site 17 in the Andaman Sea to reconstruct the variability of the South Asian monsoon during the past 60 kyr. Over this time interval εNd values changed little, generally oscillating between −7.3 and −5.3 and the Pb isotope signatures are essentially invariable, which is in contrast to a record located further northeast in the Andaman Sea. This indicates that the source of the detrital clays did not change significantly during the last glacial and deglaciation suggesting the monsoon was spatially stable. The most likely source region is the Irrawaddy river catchment including the Indo-Burman Ranges with a possible minor contribution from the Andaman Islands. High smectite/(illite + chlorite) ratios (up to 14), as well as low $^{87}Sr/^{86}Sr$ ratios (0.711) for the Holocene period indicate enhanced chemical weathering and a stronger South Asian monsoon compared to marine oxygen isotope stages 2 and 3. Short, smectite-poor intervals exhibit markedly radiogenic Sr isotope compositions and document weakening of the South Asian monsoon, which may have been linked to short-term northern Atlantic climate variability on millennial time scales.

1. Introduction

The Asian monsoon is an important component of the global climate system which directly affects the life of about half of the world's population [e.g., *An*, 2000; *Lovett*, 2010]. It is composed of two subsystems; the South Asian monsoon, also called the Indian monsoon, and the East Asian monsoon. The South Asian monsoon affects the region south of the Himalaya, Indo-China, and the South China Sea, whereas the East Asian monsoon affects China and the adjacent islands to the east. The monsoon intensity varies largely in parallel in these two subsystems [*Clift et al*., 2008]. The South Asian monsoon is further divided into South Asian winter and summer monsoons. The South Asian winter monsoon (northeast monsoon) only influences the southern peninsula of India and Sri Lanka during the northern hemisphere winter [*Kumar et al*., 2004]. In contrast, the South Asian summer monsoon (southwest monsoon) affects most regions of the Indian subcontinent and western Indo-China with peak rainfall occurring in June-September [*Pokhrel et al*., 2012].

The past variability of the South Asian monsoon has been studied using records of wind strength and associated upwelling in the Arabian Sea [e.g., *Clemens et al*., 1991; *Schulz et al*., 1998; *Caley et al*., 2011]. These records indicate a strong South Asian summer monsoon related to decreased ice volume and increased latent heat export from the southern Indian Ocean with variability linked to both the precession (23 ka) and obliquity (41 ka) cycles [e.g., *Clemens et al*., 1991; *Caley et al*., 2011]. High resolution records from the Arabian Sea [*Deplazes et al*., 2014] and Bay of Bengal [*Kudrass et al*., 2001; *Ahmad et al*., 2005; *Rashid et al*., 2011; *Marzin et al*., 2013] suggest millennial scale variability of the South Asian monsoon with a weaker monsoon during cold stadials in the North Atlantic. Studies also reported a weak monsoon during the glacial periods

over the past 280 kyr based on magnetic susceptibility, geochemical records, and sediment compositions obtained from Bay of Bengal and Andaman Sea sediments [*Colin et al*., 1998, 1999, 2006; *Rashid et al*., 2007]. A recent study of a sediment core from the Andaman Sea interpreted changes in sediment provenance to reflect a shift in the locus of the monsoon rains and changes in ocean currents [*Awasthi et al*., 2014].

Radiogenic strontium (Sr), neodymium (Nd), and lead (Pb) isotope compositions of detrital sediments are powerful tracers of sediment sources. The radiogenic Nd isotope composition provides information on the age and type of source rock, largely unaltered during weathering and sedimentary processes [e.g., *DePaolo*, 1980, 1981; *Taylor and McLennan*, 1985; *Goldstein and Jacobsen*, 1988; *McLennan and Hemming*, 1992; *Fagel et al*., 2002, 2004, 2014]. The lead isotope system has great potential for evaluating both the origin and history of sedimentary rocks. The three independent, but geochemically related, U/Th decay series, $^{238}U/^{206}Pb$, $^{235}U/^{207}Pb$, and $^{232}Th/^{208}Pb$, usually provide substantial information regarding source and geochemical evolution of the rocks [*Stacey and Kramers*, 1975; *McLennan et al*., 1993; *Dickin*, 2005]. Pb isotope compositions have also been applied for sedimentary provenance studies suggesting that the Pb isotope signature of the sources and their mixing is commonly preserved during sedimentation [e.g., *McDaniel et al*., 1994; *Hemming et al*., 1995; *von Blanckenburg and Nägler*, 2001; *Ehlert et al*., 2011; *Hu et al*., 2012; *Garçon et al*., 2013, 2014].

Detrital radiogenic Sr isotopes are sensitive to different source rocks but they are also subject to a variable degree of isotopic fractionation during weathering and transport due to large variations in the radiogenic Sr isotope composition of different mineral phases [*Tütken et al*., 2002]. Although clay-size fraction Sr isotopes cannot be used to reliably deduce sources, these data can provide useful information on weathering intensity as lower $^{87}Sr/^{86}Sr$ ratios indicate the preferential destruction of K- (and thus Rb) rich minerals in the source area and thus stronger chemical weathering [*Blum et al*., 1993, *Egli et al*., 2001, *Colin et al*., 2006; *Liu et al*., 2007]. Clay mineral assemblages also provide information on the weathering environment because the relative formation of particular clay minerals depends on the balance between physical erosion and chemical weathering in the source regions before they are eroded and transported to the ocean [*Chamley*, 1989; *Thiry*, 2000].

The Indo-Burman Ranges and surrounding regions (eastern syntaxis of the Himalayas and Tibetan Plateau) receive some of the highest summer monsoon precipitation (~1 m/month) from June to September [*Xie et al*., 2006; *Garzanti et al*., 2013]. The sediments eroded from the Indo-Burman Ranges and surrounding areas are mainly delivered by the Irrawaddy and Salween to the Andaman Sea (Figure 1). The Irrawaddy carries an annual suspended load of ~364 million tons while the Salween delivers ~164 million tons of sediment to the Andaman Sea [*Robinson et al*., 2007, and references therein]. This is approximately 35% of the suspended load delivered annually by the Ganges-Brahmaputra, the greatest globally [*Robinson et al*., 2007]. The catchment rocks of the Irrawaddy consist of Cretaceous-Cenozoic flysch of the Indo-Burman Ranges, Eocene-Miocene-Quaternary sediments of the Myanmar Central Basin, Late Precambrian, and Cretaceous-Eocene metamorphic/basic/ultrabasic rocks of the eastern syntaxis of the Himalayas (Figure 1 and Table 1) [*Bender*, 1983; *Robinson et al*., 2014; *Licht et al*., 2013]. This results in a relatively large range of Nd and Sr isotope compositions of the material supplied by the Irrawaddy (Table 1). Values measured for Irrawaddy sediments range from −10.7 to −8.3 although these are not necessarily representative for the whole river (Figure 1). The catchment rocks of the Salween consist of magmatic rock of the northern Lhasa block and Precambrian to Tertiary sedimentary, igneous and metamorphic rocks of the Shan Plateau/Sibumashau block [*Bender*, 1983].

Riverine material delivered to the Andaman sea is further distributed via the surface currents which cause the deposition of material on the slope to the south and east of the Irrawaddy and Salween (Figure 1) [*Huang et al*., 1997; *Lau and Yang*, 1997]. There are few studies of circulation in the Andaman Sea but there is general agreement that during the summer monsoon surface currents enter the Andaman Sea from the Bay of Bengal through the Preparis Channel (between Myanmar and the Andaman Islands) and the Ten Degree Channel (south of the Andaman Islands) and generally flow toward the south east forming a clockwise circulation, and exiting through the Great Channel between the Nicobar Islands and Sumatra [*Rizal et al*., 2012]. These currents carry fine-grained sediments from the Ganges in the Bay of Bengal into the Andaman sea and then pick up contributions from the Irrawaddy and Salween along their flow path and distribute these within the Andaman Sea. During the winter monsoon, the winds are reversed and the picture is less clear in the Preparis Channel where currents can apparently flow both

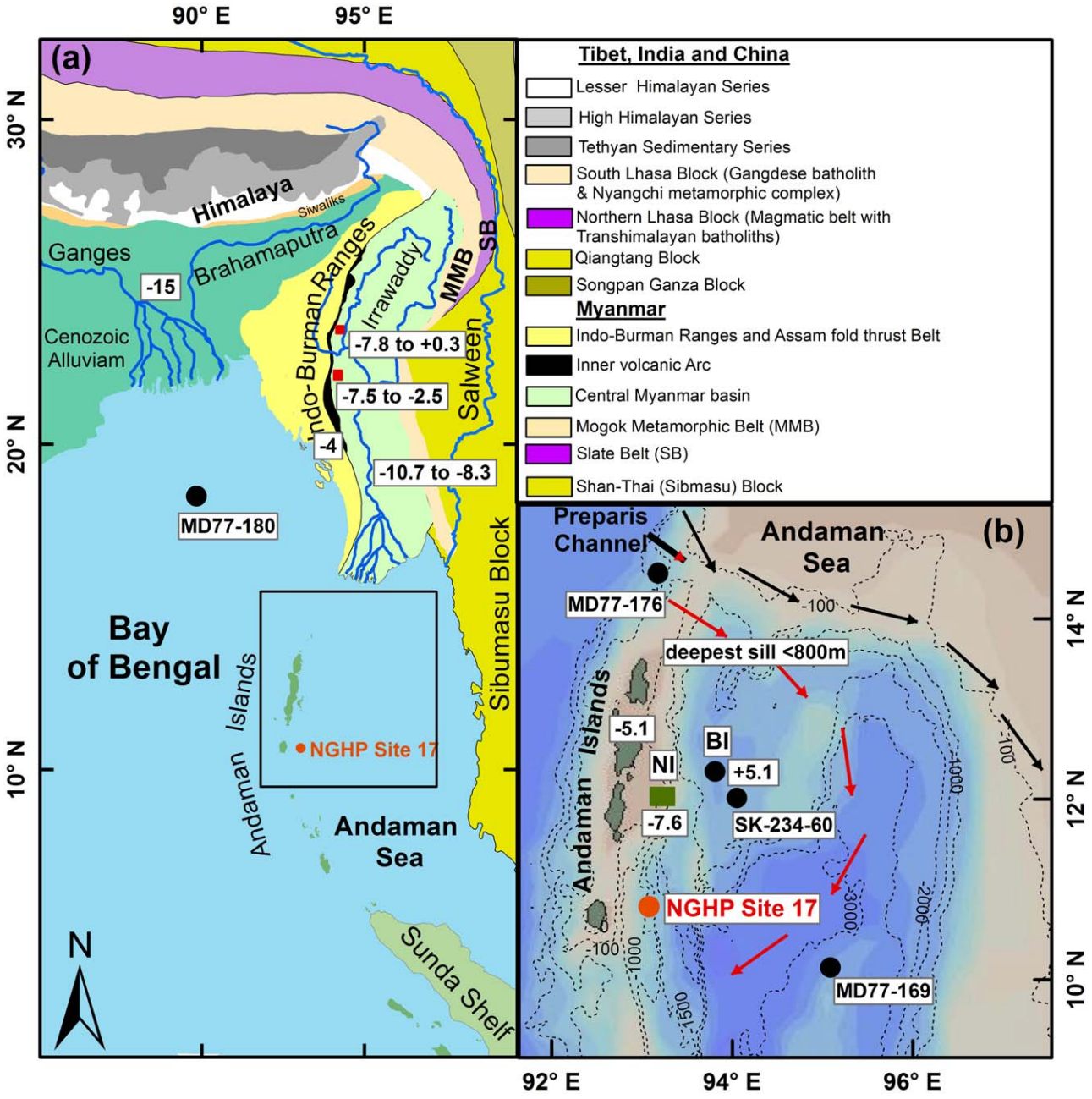

Figure 1. (a) General geological map of the Andaman Sea sediment source regions modified after *Awasthi et al.* [2014], *Robinson et al.* [2014], and *Garçon et al.* [2013]. Radiogenic isotope data are marked with numbers and detailed in Table 1. (b) Schematic bathymetric map of the Andaman Sea, modified after *IOC, IHO, and BODC* [2003] and location of NGHP Site 17 (10°45.19′N, 93°6.74′E) in the Andaman Sea. Arrows indicate directions of surface currents during the summer monsoon (black) and winter monsoon (red) periods based on the model of *Rizal et al.* [2012]. The locations of cores MD77–169, 176, and 180 were used in previous studies are shown for reference [*Colin et al.*, 1998, 1999, 2006].

eastward and westward [*Rizal et al.*, 2012]. The export of Irrawaddy material to the Bay of Bengal has been captured by the Sea WIFS satellite during December 1999 [*NASA*, 1999]. Away from the Irrawaddy, the winter surface currents generally flow to the south and south west exiting the Andaman Sea through both the Ten Degree and Great Channels [*Rizal et al.*, 2012]. Despite the seasonal changes in the currents in the Andaman Sea, surface currents will transport the material from the Irrawaddy and Salween southward year round and sources from the south can be ruled out. Therefore, the sediments deposited in the Andaman Sea record the erosion and weathering history of the Indo-Burman Ranges and Central Myanmar basin [*Colin et al.*, 1999].

Table 1. Typical Signatures of Potential Source Regions

Source Regions	Lithology and Petrography	εNd	$^{87}Sr/^{86}Sr$	$^{208}Pb/^{204}Pb$	$^{207}Pb/^{204}Pb$	$^{206}Pb/^{204}Pb$	References
Region drained by Ganges-Brahamaputra	Granites, high-grade metamorphic, low-grade metamorphic, sedimentary, and volcanic rocks	−15					*Dia et al.* [1992]
Eastern Indo-Burman Ranges	Dark gray, very fine-grained volcanic arenite of Eocene/Oligocene	−4					*Allen et al.* [2008a]
Central Myanmar basin	Pondaung formation	−7.8 to +0.3	0.705–718				*Licht et al.* [2013]
	Yaw formations	−7.5 to −2.5	0.708–0.714				*Licht et al.* [2013]
Region drained by Irrawaddy river	Cretaceous arc rocks and Triassic forearc-backarc sediments on	−10.7 and −8.3	0.713				*Colin et al.* [1999]
	metamorphic basement, Mogok schists, gneisses, and intrusives, Shan-Thai Proterozoic-Cretaceous sedimentary rocks on schist basement						*Allen et al.* [2008a]
Barren island	Volcanics	+5.2	0.703	38.402	15.560	18.256	*Luhr and Haldar* [2006]
Middle Andaman Island (12°54.22′N, 92°54.58′E)	Beach sediments	−5.1		38.969	15.350	18.799	*This study*
	Beach sediments	−5.2		38.981	15.374	18.788	*This study*
Neil Island (11°50.18′N, 93°2.1′E)	Limestone	−7.6		39.263	15.496	18.837	*This study*

The detrital fraction of marine sediments can be used to reconstruct changes in weathering, erosion, and climate on the adjacent continental landmasses [*Gingele et al*., 1999; *Thiry*, 2000; *Ehlert et al*., 2011]. In particular, the detrital clay-size fraction (<2 μm) is transported far offshore within ocean currents and is less sensitive than other grain sizes to current winnowing after deposition due to its cohesive behavior [*Fagel et al*., 2002; *Gingele and DeDeckker*, 2004; *Stumpf et al*., 2011]. Here we present the first clay-size fraction radiogenic isotope compositions (Sr, Nd, and Pb) along with the clay mineralogy of Late Quaternary Andaman Sea sediments to study the climatic and erosional history of the Indo-Burman Ranges and Central Myanmar basin. We apply the radiogenic Nd and Pb isotope compositions of the detrital clay-size fraction to reconstruct changes in the sources of clays to the Andaman Sea while using radiogenic Sr isotopes and clay minerals to infer variability in chemical weathering in the source region.

2. Materials and Methods

2.1. Core Description and Age Model

Sediment core Site 17 (10°45.19′N, 93°6.74′E) was retrieved in a water depth of 1356 m in the Andaman Sea by the Indian National Gas Hydrate Program (NGHP) using the drill ship *JOIDES Resolution* in 2006 (Figure 1) [*Collett et al*., 2008]. The site was cored to about 700 m below seafloor and preserves a late Miocene to recent stratigraphy, with a significant hiatus during the Pliocene [*Flores et al*., 2014]. Here we only focus on the upper 6.2 m to reconstruct the South Asian summer monsoon history during the last glacial and Holocene periods. There are missing portions of the core identified in Figure 2b (and all following figures), a larger one reflecting the gap between consecutive piston cores (this is an unavoidable consequence of the drilling process) and a smaller one where a whole section of core was completely sampled and removed, and thus is not available for sampling anymore. The chronology of the Site 17 sediment core (Figure 2) has been established by tuning a high resolution benthic foraminifer (*C. wuellerstorfi*) oxygen isotope record to the LR04 benthic oxygen isotope stack [*Lisiecki and Raymo*, 2005] using *Analyseries* [*Paillard et al*., 1996]. The extended benthic and planktonic stable isotope records of this core comprising the past 2 million years will be discussed in detail in a separate publication (Gebregiorgis et al., manuscript in preparation). The age model was further constrained by five Accelerator Mass Spectrometry (AMS) ^{14}C dates on planktonic foraminifera (Table 2). The radiocarbon dates were corrected for marine reservoir ages determined locally by *Southon et al*. [2002]. The oxygen isotopes of mixed layer dwelling planktic foraminifer *G. sacculifer* supports the benthic foraminifer (*C. wuellerstorfi*)-based age model. Sedimentation rates were largely invariant ranging between 10.2 and 11.7 cm/kyr over the past 60 kyr, with the exception of a short interval of somewhat increased sedimentation rates (16 cm/kyr). The sediments in the upper 6.2 m of the core are composed of

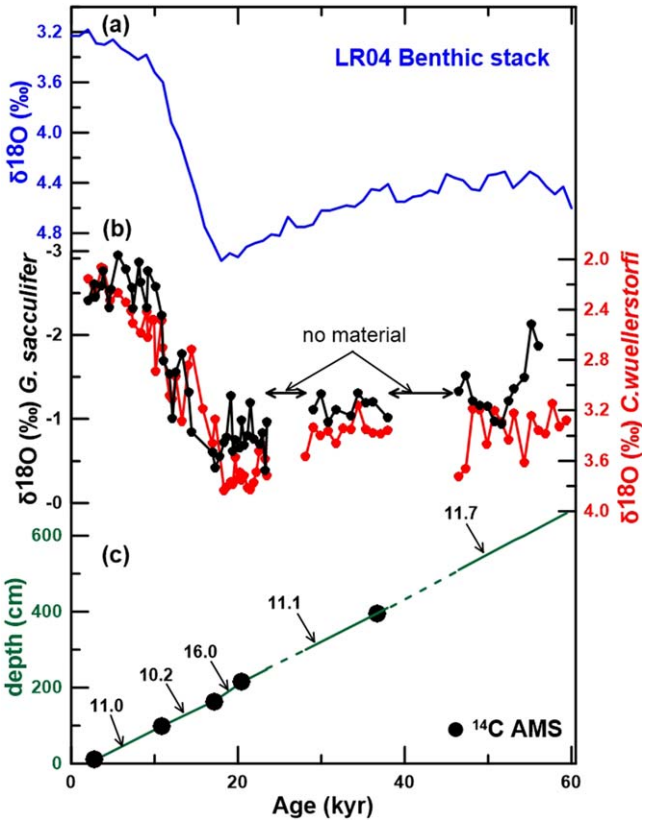

Figure 2. (a) LR04 global benthic $\delta^{18}O$ reference stack; (b) $\delta^{18}O$ of benthic foraminifera (*C. wuellerstorfi*) and planktonic foraminifera (*G. sacculifer*) from NGHP Site 17. The stratigraphy of the core was established with five ^{14}C AMS dates, the youngest Toba ash, and tuning of the benthic oxygen isotope record to the LR04 stack [*Lisiecki and Raymo*, 2005]. This correlation was established graphically using *Analyseries* [*Paillard et al.*, 1996]. (c) depth (cm) versus age (kyr) plot showing sedimentation rates (cm/kyr) between radiometric control points.

foraminifera-rich nannofossil oozes [*Collett et al.*, 2008] with an average bulk $CaCO_3$ content of 25 wt % [*Johnson et al.*, 2014]. The average TOC content within this interval is 1.0 wt % and bulk $\delta^{13}C_{org}$ measurements ($-20‰$ on average) are consistent with a dominance of marine organic matter [*Johnson et al.*, 2014]. The noncarbonate sediment fraction is dominated by clay minerals [*Phillips et al.*, 2014; this study]. Volcanic ash layers are abundant throughout the record below ~8 mbsf [*Collett et al.*, 2008; *Rose et al.*, 2014]. The uppermost bioturbated volcanic ash bed at 8.39–8.46 mbsf is from the most recent Toba eruption at 75 ± 0.9 ka [*Mark et al.*, 2014] and its depth in the core confirms our age model. This is based on binary relationships of the major and minor element geochemical compositions obtained by electron microprobe (EMP) analysis, which agree with previous analyses of the Toba ash [*Smith et al.*, 2011] (supporting information Figure S1).

2.2. Methods

In total, 27 samples (Table 3) were selected for the analysis of radiogenic Sr and Nd isotopes and 16 samples for Pb isotope analysis of the clay-size fraction. The same set of samples (27 samples) was analyzed for clay mineral assemblages. In addition, sedimentary rock and beach sediment samples obtained from Neil Island and Middle Andaman Island were analyzed to constrain the influence of the Andaman Islands as a source of sedimentary material. To separate the clay-size fraction from the bulk sediments, we followed the procedure of *Stumpf et al.* [2011]. Sediments samples were first freeze dried and the >63 μm size fraction was separated by wet sieving. The <63 μm size fractions were further processed to separate the clay-size fraction (<2 μm). In a first preparation step, carbonates and organic matter were removed with acetic acid and hydrogen peroxide, followed by a triple rinse with deionized water. A centrifuge based Atterberg method was used to separate the clay-size fraction (<2 μm). The required settling times were calculated with the freely available software

Table 2. Conventional AMS ^{14}C Ages on Hand Picked Planktonic Foraminifera From NGHP Site 17, Together With the Calibrated Calender Ages[a]

Site	Core	Type	Section	Depth (cm)	Conventional ^{14}C Age (Year ± 1σ)	Calibrated Age (Year BP)
NGHP17	1	H	1	10	3,090 ± 25	2,734–2859
NGHP17	1	H	1	99	10,000 ± 35	10,742–11,059
NGHP17	1	H	2	163	14,550 ± 25	16,957–17,340
NGHP17	1	H	2	216	17,450 ± 70	20,255–20,693
NGHP17	1	H	3	396	33,300 ± 25	36,406–37,087

[a]AMS ^{14}C measurements were carried out at the Woods Hole Oceanographic Institute, USA. The radiocarbon dates were corrected, by using Calib 7.0 [*Stuiver et al.*, 2014], for marine reservoir ages (Delta $R = 63.0$) determined locally by *Southon et al.* [2002].

Table 3. Nd, Sr, and Pb Isotope Data of NGHP Site 17 With 2σ error in Parentheses, Measured on <2 μm Size Fraction

Site	Core	Type	Section	Depth (cm)	Age (kyr)	εNd (±0.50)	$^{87}Sr/^{86}Sr$ (±0.00004)	$^{208}Pb/^{204}Pb$ (±0.0068)	$^{207}Pb/^{204}Pb$ (±0.0030)	$^{206}Pb/^{204}Pb$ (±0.0022)
NGHP17	1	H	1	10	2.92	−7.1	0.7126			
NGHP17	1	H	1	20	3.81	−5.8	0.7124	39.221	15.723	18.811
NGHP17	1	H	1	40	5.61	−6.8	0.7119			
NGHP17	1	H	1	60	7.41	−6.2	0.7114	39.189	15.719	18.791
NGHP17	1	H	1	70	8.31	−5.7	0.7116			
NGHP17	1	H	1	100	11.01	−5.6	0.7112			
NGHP17	1	H	1	124	13.30	−6.3	0.7126	39.134	15.711	18.781
NGHP17	1	H	2	150	15.77	−5.8	0.7121	39.116	15.707	18.763
NGHP17	1	H	2	162	16.91	−6.0	0.7121			
NGHP17	1	H	2	186	18.61	−5.8	0.7121	39.145	15.711	18.770
NGHP17	1	H	2	198	19.40	−5.6	0.7119			
NGHP17	1	H	2	202	19.67	−5.3	0.7124	39.135	15.705	18.774
NGHP17	1	H	2	214	20.46	−6.1	0.7130	39.121	15.701	18.774
NGHP17	1	H	2	226	21.49	−5.6	0.7122	39.118	15.706	18.761
NGHP17	1	H	2	238	22.57	−5.9	0.7118			
NGHP17	1	H	2	242	22.93	−5.7	0.7122	39.173	15.715	18.784
NGHP17	1	H	3	300	28.13	−6.3	0.7138	39.148	15.717	18.762
NGHP17	1	H	3	310	29.03	−5.7	0.7133			
NGHP17	1	H	3	340	31.72	−6.1	0.7119	39.112	15.703	18.756
NGHP17	1	H	3	370	34.41	−6.6	0.7126	39.192	15.709	18.808
NGHP17	1	H	3	390	36.20	−6.2	0.7122			
NGHP17	1	H	3	400	37.08	−5.3	0.7148	39.159	15.710	18.785
NGHP17	2	H	1	520	47.02	−5.7	0.7124	39.055	15.702	18.748
NGHP17	2	H	2	570	51.29	−6.6	0.7119			
NGHP17	2	H	2	590	52.42	−7.3	0.7139	39.115	15.704	18.757
NGHP17	2	H	2	610	54.87	−6.9	0.7120			
NGHP17	2	H	2	620	55.72	−6.7	0.7126	39.153	15.709	18.788

SediCalc [*Krumm*, 2006]. The <2 μm size fraction was confirmed by analyzing a subset of samples with a laser diffraction particle size analyzer (Beckman Coulter LS I3 320). Finally, the size separated samples were freeze-dried before total dissolution or XRD analysis.

About 50 mg of the dried clay-size fraction were completely dissolved using a mixture of concentrated HF-HNO_3-$HClO_4$. The separation and purification of Sr, Nd, and Pb followed previously published procedures for Sr [*Bayon et al*., 2002; *Horwitz et al*., 1992], Nd [*Barrat et al*., 1996; *Cohen et al*., 1988; *Le Fèvre and Pin*, 2005], and Pb [*Galer and O'Nions*, 1989; *Lugmair and Galer*, 1992]. Finally, Sr, Nd, and Pb isotopes were measured on a Nu Plasma MC-ICP-MS at GEOMAR, Kiel. Measured Sr isotope ratios were interference (^{86}Kr, ^{87}Rb) and mass bias corrected using $^{86}Sr/^{88}Sr = 0.1194$ [*Steiger and Jäger*, 1977]. $^{87}Sr/^{86}Sr$ results were normalized to the accepted value for NIST NBS987 = 0.710245. The 2σ reproducibility for the NIST NBS987 standard was ±0.00004. Repeated processing and analysis of USGS marine sediment reference material MAG-1 (n = 7) gave a mean $^{87}Sr/^{86}Sr$ value of 0.722973 ± 0.00002 which agrees well with the value (0.722739) reported by *Nath et al*. [2009]. $^{143}Nd/^{144}Nd$ ratios were mass-bias corrected to $^{146}Nd/^{144}Nd = 0.7219$ and normalized to the accepted value of the JNdi-1 standard of 0.512115 [*Tanaka et al*., 2000]. Repeated measurements of an in-house Nd standard "SPEX" gave a reproducibility of ±0.50 (2σ) εNd. Repeated processing and analysis of reference material MAG-1 (n = 19) gave a mean εNd value of −11.19 ± 0.2 which agrees well (i.e., within 36 ppm) with the values reported by *Nath et al*. [2009]. A standard-sample bracketing method [*Albarède et al*., 2004] was used to determine the Pb isotope ratios. All analyzed Pb isotope ratios were then normalized to the accepted value of the NBS981 standard of $^{208}Pb/^{204}Pb = 36.7219 \pm 0.0044$, $^{207}Pb/^{204}Pb = 15.4963 \pm 0.0016$, and $^{206}Pb/^{204}Pb = 16.9405 \pm 0.0015$ [*Abouchami et al*., 1999]. The 2σ reproducibility for the NIST NBS981 standard was ±0.0068, ±0.0030, and ±0.0022 for $^{208}Pb/^{204}Pb$, $^{207}Pb/^{204}Pb$, and $^{206}Pb/^{204}Pb$, respectively. The MAG-1 standard and blanks were processed and measured together with the clay fraction samples. Blanks were typically below 200 pg so that blank contributions to the Pb analyses can be neglected. Repeated processing and analysis of MAG-1 (n = 4) gave a mean value ±2 standard deviations of 38.810 ± 0.011, 15.656 ± 0.003, and 18.861 ± 0.002 for $^{208}Pb/^{204}Pb$, $^{207}Pb/^{204}Pb$, and $^{206}Pb/^{204}Pb$, respectively. These Pb isotope values agree well with those previously for MAG-1 [*Nath et al*., 2009].

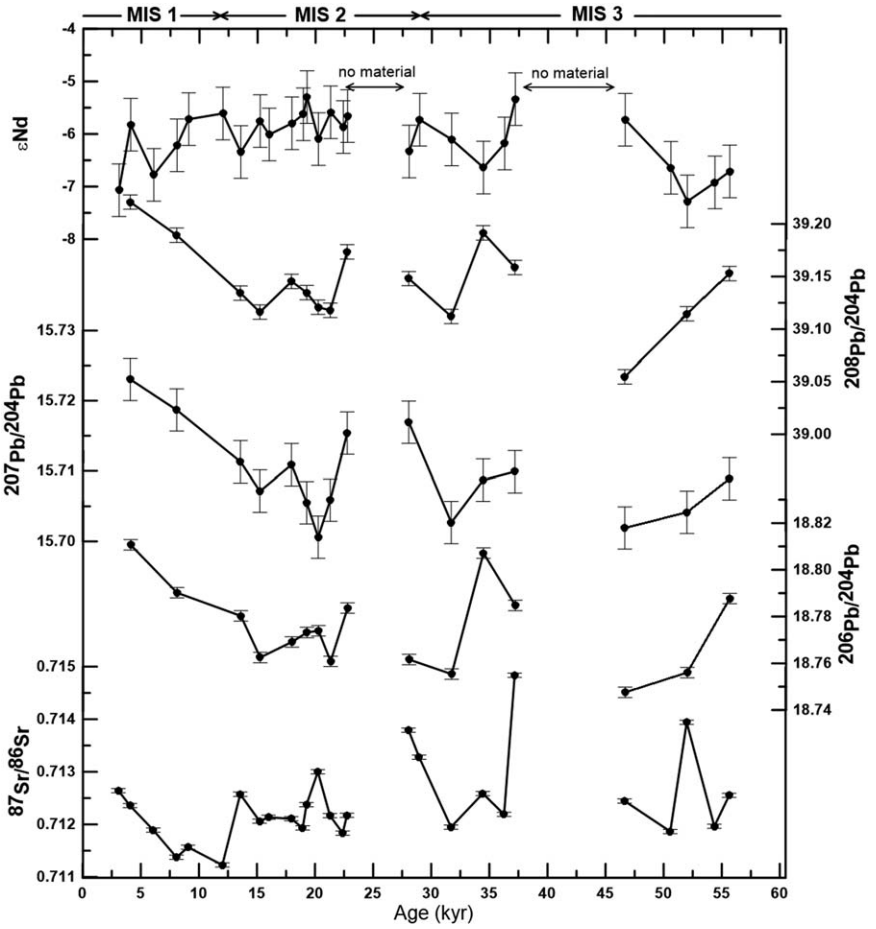

Figure 3. Nd, Pb, and Sr isotope compositions of clays. MIS 1, 2, and 3 denote the marine isotopic stages. Error bars represent the 2σ uncertainty estimated by repeated measurement of an in-house standard during the sample measurements.

For the clay mineral analyses, the same set of samples taken for the radiogenic isotope compositions was used. The carbonate- and organic carbon-free clay-size fraction (<2 μm) was suspended in an ultrasonic bath and placed on 0.2 μm filters by applying a vacuum below the filters. The XRD runs were performed following glycol-dehydration for 24 h. The analyses were conducted using a Phillips X-Ray diffractometer (PW series) with CoKα radiation and a Ni filter under a voltage of 40 kV and an intensity of 35 mA. The relative amount of each clay mineral was estimated according to the position of the (0 0 1) series of the basal reflections on the XRD diagrams, i.e., smectite (0 0 1) at 17 Å, illite (0 0 1) at 10 Å, kaolinite (0 0 1) and chlorite (0 0 2) at 7 Å. Kaolinite and chlorite were discriminated according to the relative proportions deduced from the ratios of the 3.57 and 3.54 Å peak areas. One sample was measured three times and the reproducibility of the semiquantitative clay mineral analysis was around $\pm$2%.

3. Results

3.1. Sr, Nd, and Pb Isotope Compositions

Sr, Nd, and Pb isotope compositions measured on the clay-size fraction are provided in Table 3 and are displayed in Figure 3. Nd isotope results are expressed as εNd values corresponding to the deviation of the measured $^{143}Nd/^{144}Nd$ ratios of a sample from that of the chondritic uniform reservoir (CHUR = 0.512638), multiplied by 10,000 [*Jacobsen and Wasserburg*, 1980]. The εNd values range from -7.3 to -5.3 for the last glacial period and -7.1 to -5.6 for the Holocene. The average εNd values of -6.1 and -6.2 are indistinguishable for these periods. The clay fraction $^{208}Pb/^{204}Pb$, $^{207}Pb/^{204}Pb$, and $^{206}Pb/^{204}Pb$ ratios are also similar for the last glacial and the Holocene periods (Table 3 and Figure 4). In contrast, $^{87}Sr/^{86}Sr$ ratios are generally more radiogenic during the last glacial period (0.712–0.715) than during the Holocene (0.711–0.712).

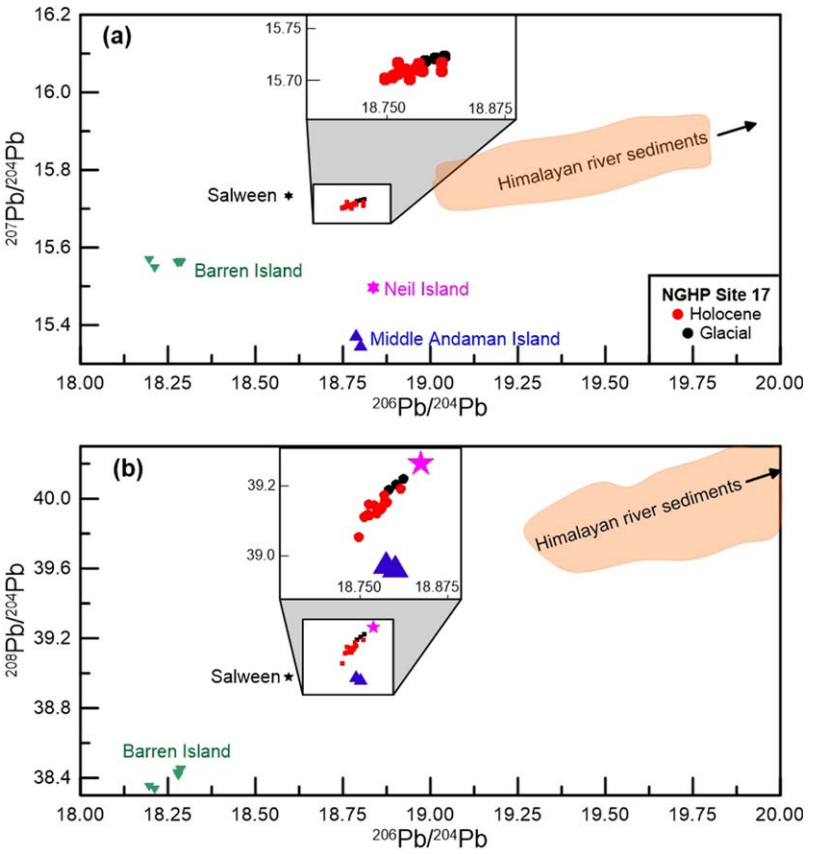

Figure 4. (a) $^{207}Pb/^{204}Pb$-$^{206}Pb/^{204}Pb$ and (b) $^{208}Pb/^{204}Pb$-$^{206}Pb/^{204}Pb$ diagrams for NGHP Site 17 clays and potential source areas in the north eastern Indian Ocean. The Pb isotope compositions of Himalayan river flood plain sediments are from *Garçon et al.* [2013], Salween from *Millot et al.* [2004], and Barren Island data are from *Luhr and Haldar* [2006].

3.2. Clay Mineral Assemblages

The results of the clay mineral analyses are listed in Table 4 and shown in Figure 5. Smectite, illite, chlorite, and kaolinite are present in all analyzed samples. Smectite is the dominant clay mineral ranging from 62.5% to 85.5% (average ~77%) in the glacial and 81.8% to 84.2% (average ~83%) for the Holocene sediments. Illite contents vary from 2.3% to 8.2% (average ~5%) during the last glacial and 1.1% to 3.5% (average ~3%) during the Holocene. Chlorite contents vary from 5.0% to 21.2% (average ~10%) and 4.5% to 7.6% (average 6%) during the glacial and Holocene periods, respectively. The abundance of kaolinite was slightly higher during the glacial period (6.6–13.1%; average 8.8%) than during the Holocene (6.3–9.8%; average 8.0%) and varied in parallel with the illite and chlorite abundances and is mostly a consequence of dilution with smectite.

4. Discussion

4.1. Source of the Andaman Sea Sediments

Neodymium isotope signatures can provide information about the sources of the clays deposited in the Andaman Sea and here, for the first time in this area, we employ Pb isotopes as an additional constraint. Although Pb isotopes can be affected by incongruent weathering, especially under glacial conditions [*von Blanckenburg and Nägler*, 2001], this is unlikely to have occurred in the tropical catchments draining into the Andaman Sea. Additionally, *Garçon et al.* [2013, 2014] found that the Pb isotope compositions of the clay-size fraction of detrital sediments reflects that of the source area because most of the lead in the clays was initially present in crustal rocks and not from heavy minerals with markedly different compositions. Hence, the Pb isotope compositions of clays can, with some caution, be used to constrain the sources of

Table 4. Clay Mineral Abundances in Weighted Peak Area Percentage[a]

Site	Core	Type	Section	Depth (cm)	Age (kyr)	Smectite (%)	Illite (%)	Kaolinite (%)	Chlorite (%)	Smectite/ (Illite + Chlorite)
NGHP17	1	H	1	10	2.92	82	4	8	7	7.8
NGHP17	1	H	1	20	3.81	84	1	9	6	12.3
NGHP17	1	H	1	40	5.61	84	3	6	8	8.3
NGHP17	1	H	1	60	7.41	84	1	10	5	14.0
NGHP17	1	H	1	70	8.31	83	3	7	6	8.6
NGHP17	1	H	1	100	11.01	82	3	8	8	7.9
NGHP17	1	H	1	124	13.30	85	3	7	5	11.1
NGHP17	1	H	2	150	15.77	79	4	8	9	6.3
NGHP17	1	H	2	162	16.91	84	4	7	5	9.2
NGHP17	1	H	2	186	18.61	85	2	7	5	11.4
NGHP17	1	H	2	198	19.40	82	2	7	9	7.5
NGHP17	1	H	2	202	19.67	83	3	7	7	7.9
NGHP17	1	H	2	214	20.46	78	4	9	10	5.8
NGHP17	1	H	2	226	21.49	66	7	13	14	3.1
NGHP17	1	H	2	238	22.57	74	5	10	11	4.6
NGHP17	1	H	2	242	22.93	78	4	9	9	5.9
NGHP17	1	H	3	300	28.13	74	5	10	11	4.5
NGHP17	1	H	3	310	29.03	80	4	7	8	6.4
NGHP17	1	H	3	340	31.72	81	3	9	7	8.0
NGHP17	1	H	3	370	34.41	77	5	9	10	5.2
NGHP17	1	H	3	390	36.20	81	4	8	7	7.0
NGHP17	1	H	3	400	37.08	70	7	10	13	3.6
NGHP17	2	H	1	520	47.02	80	4	7	9	6.5
NGHP17	2	H	2	570	51.29	79	5	8	8	6.1
NGHP17	2	H	2	590	52.42	66	8	13	13	3.1
NGHP17	2	H	2	610	54.87	78	5	9	8	6.1
NGHP17	2	H	2	620	55.72	71	6	10	12	3.8

[a]The reproducibility of the semiquantitative clay mineral analysis is about ±2%.

the sediments in the Andaman Sea. This is supported by radiogenic isotope results obtained from the clay-size fraction under similar environmental conditions in the eastern Indian Ocean [*Ehlert et al*., 2011].

The εNd values of NGHP Site 17 clays (average εNd = −6.2) are significantly more radiogenic than the published data for Irrawaddy River sediments (εNd = −8.3) [*Allen et al*., 2008a], surface sediments off the Thailand coast (εNd = −9) [*Dia et al*., 1992], and bulk sediment compositions obtained from core MD77–169 in the Andaman Sea (εNd = −9.5 to −10.5) [*Colin et al*., 1999, 2006]. On the other hand, the εNd values of Site 17 are less radiogenic than those of the clay fraction of Middle Andaman Island beach sediments (εNd = −5.1). The fact that the data for the two Andaman Island samples studied straddle the range of values found in the Site 17 sediments suggests that mainly local sources may have provided the clay-size fraction. However, there are no major rivers on the Andaman Islands that could provide a significant amount of sediments to the Andaman Sea. Instead the Andaman Islands consist of uplifted accretionary prism materials [*Allen et al*., 2008b; *Garzanti et al*., 2013] originating from uplifted Bengal/Nicobar submarine fan sediments. The sediments of the eastern side of the Andaman Islands show mineralogical similarities with modern Irrawaddy River sediments revealing significant contributions from mafic/ultramafic rocks of the Burma arc-trench system [*Garzanti et al*., 2013]. Our measurement of the clays from a limestone sample (Neil Island) from the Archipelago Group of Miocene to Pliocene age [*Allen et al*., 2008a] also gives a Nd isotope composition (εNd = −7.6) similar to that of the Site 17 clays. There are currently only two Nd isotope measurements of Irrawaddy river sediments, at least one of which is from the upper reaches that may not be representative of the entire catchment [*Allen et al*., 2008b]. Fluvial clastic sedimentary rocks from the Central Myanmar basin display a wide range of Nd isotope compositions from −7.8 to +0.3 [*Licht et al*., 2013] and it is thus feasible that the Site 17 clays are sourced entirely from the Irrawaddy catchment. The fact that Site 17 clays are somewhat more radiogenic than the existing data for the Irrawaddy river implies that there has also been a small contribution from a more radiogenic source such as Barren Island. The only active volcano in the region, Barren Island consists of highly radiogenic (average εNd = +5.2) Quaternary basalts [*Luhr and Haldar*, 2006]. A simple two component mass balance, using εNd = −8.3 as the Irrawaddy River endmember and εNd = +5.2 as the Barren Island endmember, suggests a maximum of only 15% of the clays are from a radiogenic source like Barren Island. Despite the dearth of data for the Irrawaddy

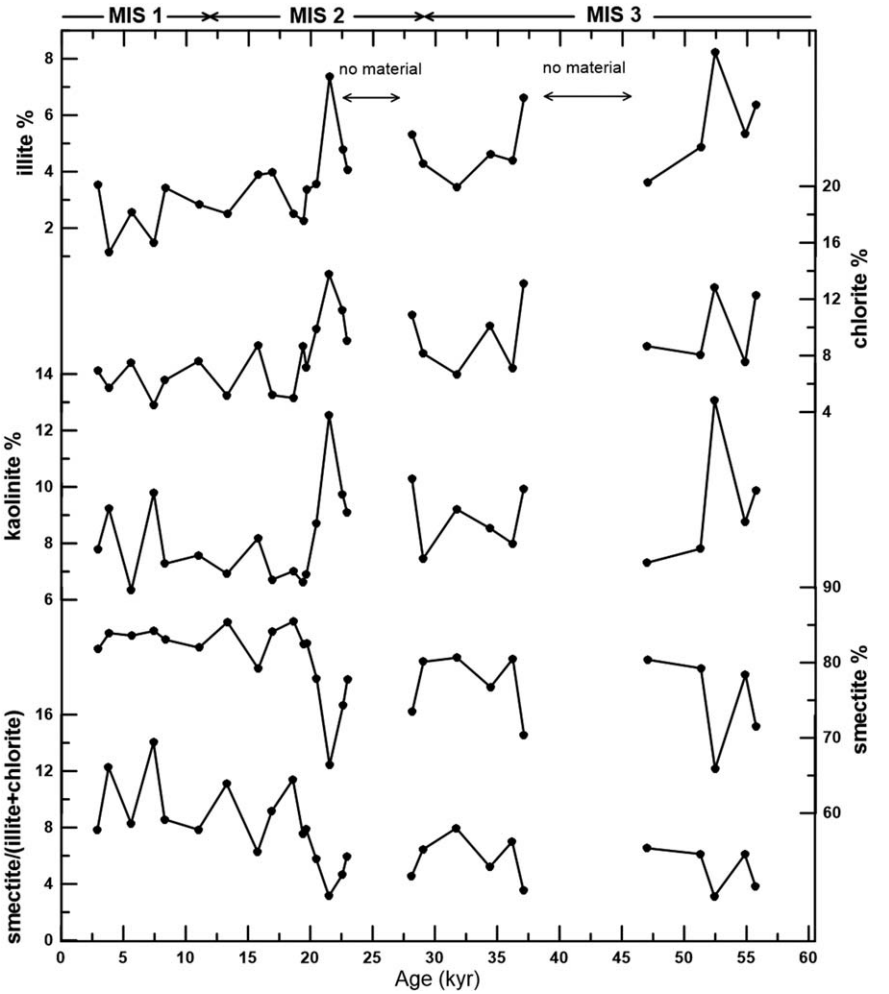

Figure 5. Clay mineral assemblages and smectite/(illite + chlorite) ratios during the last 60 kyr.

catchment, the lack of variability in the NGHP Site 17 Nd isotope compositions suggests a stable source of clays transported to the Andaman Sea during the past 60 kyr.

Binary relationships of $^{208}Pb/^{204}Pb$-$^{206}Pb/^{204}Pb$ and $^{207}Pb/^{204}Pb$-$^{206}Pb/^{204}Pb$ also suggest a consistent source of clay-sized fraction to the Andaman Sea during the last glacial and Holocene periods (Figure 4). The Pb isotope mixing relationships suggest that the Barren Island volcanic rocks may be a possible end-member source [*Luhr and Haldar*, 2006] but cannot have contributed sufficient amounts of sediment to explain the observed clay fraction signatures. The $^{207}Pb/^{204}Pb$-$^{206}Pb/^{204}Pb$ data also clearly show that the Andaman Islands cannot have been a significant contributor of clays to the core location. The Pb isotope compositions of the Andaman Sea clays suggest they may contain components of Himalayan river [*Garçon et al*., 2013] and Salween river sediments [*Millot et al*., 2004]. However, these Pb isotope fields are not close enough to allow for a significant contribution from these rivers. Although to date, there are no Pb isotope data available from the Indo-Burman Ranges or Irrawaddy river sediments, based on the exclusion of other sources and together with the Nd isotopes, we suggest the Irrawaddy catchment (Indo-Burman Ranges and Central Myanmar basin) as the main source of the detrital sediments.

Together the Nd-Pb isotope compositions (supporting information Figure S2), therefore suggest a major and stable contribution from the Indo-Burman Ranges and Central Myanmar basin to the Andaman Sea clays resulting in little downcore variation since 60 ka. This is also in agreement with previous studies showing that the inputs to the Andaman Sea did not vary strongly over time [*Colin et al*., 1999, 2006]. However, a detrital Nd isotope record obtained on sediment core (SK-234-60), located to the northeast of NGHP Site 17

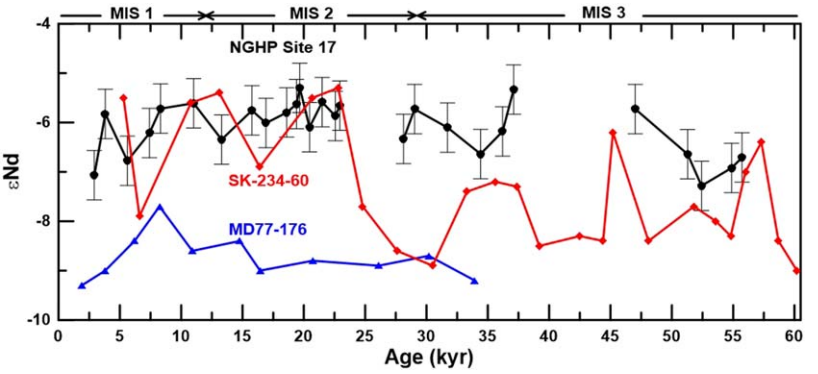

Figure 6. Nd isotope time series of NGHP Site 17 clays compared with cores SK-234-60 [*Awasthi et al*., 2014] and MD77–176 [*Colin et al*., 2006].

in the Andaman Sea, shows a much larger range of downcore isotopic variations (Figure 6) [*Awasthi et al*., 2014]. It was suggested that this variability in the relative contributions from different source areas was related to changes in the monsoon locus during some interstadials and the Holocene [*Awasthi et al*., 2014]. The core used in that study experienced variable sedimentation rates, which reached minimum values during the last glacial period (for details see Figure 2 of *Awasthi et al*. [2014]) suggesting the variability may be related to transport processes. These changes in source contributions to core SK-234-60 (Figure 6) were most likely caused by ocean surface currents that transported sediments of Ganga-Brahamaputra origin from the Bay of Bengal across the Preparis Channel to the Andaman Sea (Figure 1). These transport processes affecting the northern Andaman Sea obviously did not influence sedimentation at NGHP Site 17 and other locations further south (MD77–169) as evident from their nearly constant Nd-Pb isotope compositions.

4.2. Clay Mineral Assemblages: A Tracer for Chemical Weathering

Illite and chlorite are considered primary detrital clay minerals [*Chamley*, 1989]. A high abundance of these minerals reflects decreased hydrolytic processes during continental weathering and increased rock erosion under cold and/or arid climatic conditions. In the case the Indo-Burman Ranges, illite and chlorite have most likely been produced by the physical erosion of igneous, metamorphic, and sedimentary parent rocks [*Bender*, 1983; *Allen et al*., 2008a]. An increase in illite and chlorite abundances during the last glacial period therefore suggests increased physical erosion in the upper reaches of the Irrawaddy basin. Kaolinite is considered a secondary clay mineral formed under humid and warm climatic conditions by intense chemical weathering [*Chamley*, 1989]. However, our results show that the kaolinite content displays a pattern similar to illite and chlorite in all studied samples suggesting dilution with variable amounts of the dominant smectite (Figure 5). Given that the sedimentation rates during the observed period of time were essentially constant, this suggests that also the input fluxes of illite, chlorite, and kaolinite were higher during the glacial. Smectite is also a secondary clay mineral. Warm and humid regions with less leaching predominantly produce smectite-rich soils as a residue of weathering of aluminosilicates and ferromagnesian silicate [*Chamley*, 1989]. In addition, the chemical weathering of basaltic rocks under various climatic conditions will produce smectite [*Griffin et al*., 1968]. The high content of smectite found at Site 17 is most likely the weathered residue of the volcanic dykes and ophiolitic formations of the late Mesozoic-Cenozoic volcanic arc of the Indo-Burman Ranges and Central Myanmar basin [*Bender*, 1983; *Licht et al*., 2013]. In general, the smectite content of the studied samples is similar to the clay mineral records obtained in the eastern Andaman Sea [*Colin et al*., 1999] but higher than those of the Irrawaddy River-dominated coastal surface sediments [*Bunsomboonsakul et al*., 2010]. This might result from particle fractionation as smectite dominates the smallest clay mineral size fraction [*Kurian et al*., 2008] that is consequently transported further away from the coastal source areas to the core site. A significant influence (>15%) of the local Barren Island basalts [*Luhr and Haldar*, 2006] has been ruled out based on the Nd isotope composition of the clays.

Assuming local sources and transport effects have been minimal, the clay mineral assemblage and secondary smectite to primary illite + chlorite ratios (smectite/(illite + chlorite)) recorded in the Andaman Sea can

be used as a proxy of chemical weathering intensity. This will reflect the balance between physical erosion and chemical weathering in the Irrawaddy catchment (IBR, Central Myanmar basin). The smectite content and smectite/(illite + chlorite) ratios follow the glacial-interglacial cyclicity with significantly lower ratios during the glacial period and higher ratios during the Holocene (Figure 5). Although the resolution of our record (~2 kyr) makes it difficult to clearly resolve millennial scale variability, there are clear indications of lower smectite content and lower smectite/(illite + chlorite) ratios during times associated with the Heinrich intervals. This implies that more intense physical erosion prevailed in the Irrawaddy catchment during the colder glacial and stadial periods although the relative timing is difficult to interpret.

4.3. $^{87}Sr/^{86}Sr$ Ratios Tracing the Intensity of Chemical Weathering

The Sr isotope composition of detrital sediments is predominantly controlled by grain-size sorting during transport, changes in the source region, and the intensity of chemical weathering on land [*Meyer et al*., 2011; *Tütken et al*., 2002]. We have separated the clay-size fraction (<2 μm) to minimize the effect of sediment sorting during transport, acknowledging that some sorting of the fine fraction has most likely already occurred in the catchment of the river and during riverine transport. The Nd and Pb isotope compositions indicate essentially constant source areas over the past 60 kyr suggesting little influence of source region changes on the studied sediment composition during this period. Therefore, the Sr isotope compositions of the carbonate and organic matter free clay fraction indicate changes of the incongruent weathering of the silicate rocks in the source region [*Taylor and Blum*, 1995]. *Colin et al*. [2006] demonstrated the variation of Sr isotope compositions in Andaman Sea sediments is independent of the source of the sediments, the distance from the source river mouth, and grain-size sorting effects. These authors further suggested that an increase in $^{87}Sr/^{86}Sr$ ratios corresponded to the intensification of physical erosion in the Irrawaddy River catchment caused by enhanced release of unaltered minerals such as mica with high $^{87}Sr/^{86}Sr$ ratios. The Sr isotopic composition of the clay-size fraction from Site 17 is lower than that of the bulk sediments in the Andaman Sea [*Colin et al*., 2006]. This deviation is most likely simply caused by minor contributions from less radiogenic sources (e.g., Barren Island, Table 1). The trend displayed by the Sr isotope composition of clays and the bulk sediments is similar between the Holocene and glacial periods with glacial sediments characterized by higher $^{87}Sr/^{86}Sr$ ratios than Holocene sediments.

The clay $^{87}Sr/^{86}Sr$ record displays a glacial-interglacial variability similar to the clay mineral assemblages (Figure 7), indicating more intense physical erosion during glacial period. Although the record is too coarse in resolution and the age model is not precise enough to unambiguously resolve millennial scale variability, higher $^{87}Sr/^{86}Sr$ ratios generally appear to have been associated with cold stadials, in particular Heinrich events H3, H4, and H5a. Consistent with the clay mineral variations this also points to enhanced physical erosion under drier conditions and relatively low chemical weathering intensity. However, unlike the clay mineral composition, the $^{87}Sr/^{86}Sr$ ratios of the clays did not change during Heinrich stadial H1, suggesting a lower sensitivity of the Sr isotopes to weathering intensity compared to the clay mineral assemblages (Figure 7) under full glacial conditions. This is most likely a consequence of the clay mineral assemblages and Sr isotope compositions being affected by weathering intensity and source rock composition in different ways, and not in a linear manner.

4.4. Variability of the South Asian Monsoon in the Irrawaddy Catchment

The Site 17 clay fraction documents the variability of the South Asian summer monsoon during the last glacial and Holocene (Figure 7). An increased chemical weathering intensity during the Holocene period indicates a stronger South Asian summer monsoon over the Irrawaddy catchment, consistent with other proxy records obtained in the Andaman Sea [*Colin et al*., 1999, 2006]. *Rashid et al*. [2007, 2011] presented a millennial-scale salinity record from core RC12-344 in the Andaman Sea that shows lowered sea surface salinity caused by increased South Asian summer monsoon rainfall during the early Holocene. An increase in continental wetness during the Holocene has also been inferred from the $\delta^{18}O$ of *G. ruber* from the northern Andaman Sea [*Marzin et al*., 2013]. The higher $^{87}Sr/^{86}Sr$ ratios since ~6 ka were most likely caused by a weakening of the South Asian summer monsoon following a maximum in monsoon intensity during the early Holocene.

The Andaman Sea clay record also suggests relatively rapid changes in physical erosion and chemical weathering as inferred from the variations in the smectite/(illite + chlorite) and Sr isotope ratios. Higher physical erosion occurred around ~16, ~22, ~29, and ~37 ka. Although our age model and sampling resolution do

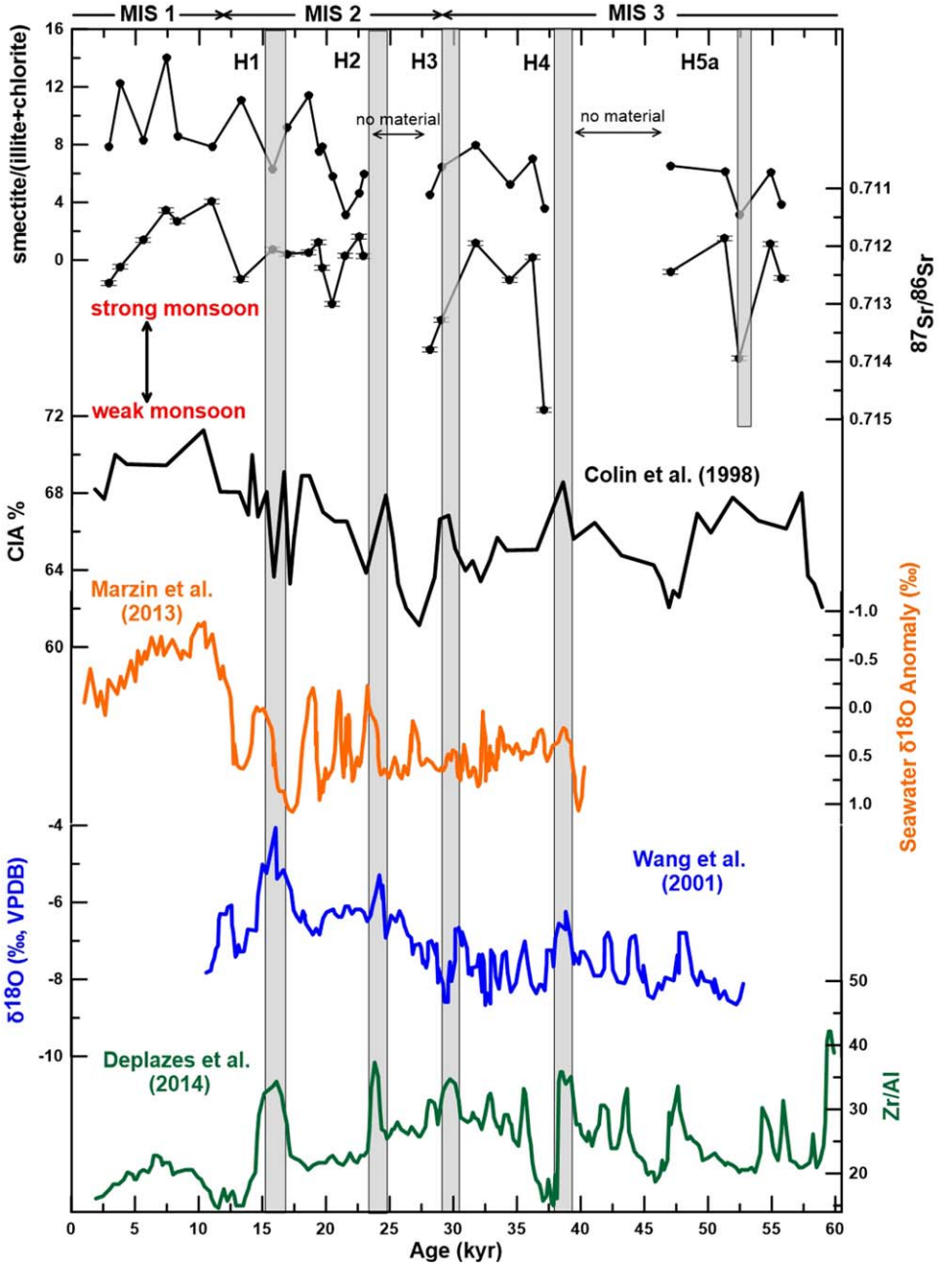

Figure 7. Smectite/illite + chlorite, Sr isotope composition from NGHP Site 17 (cf. Figures 3 and 5) compared with the Chemical Index of Alteration (CIA) [*Colin et al.*, 1998] of Core MD77–180 from the Bay of Bengal, seawater δ^{18}O anomaly [*Marzin et al.*, 2013] of Core MD77–169 from the Andaman Sea, δ^{18}O records [*Wang et al.*, 2001] of Hulu cave stalagmites and the Zr/Al record [*Deplazes et al.*, 2014] of Core 289KL from the Arabian Sea. MIS 1, 2, and 3 denote the marine isotopic stages and the vertical bars show the ages of Heinrich events H1–H4 [*Hemming*, 2004], as well as of Heinrich event H5a [*van Kreveld et al.*, 2000; *Rashid et al.*, 2003].

not permit unambiguous comparison, there seems to be a broad correspondence to the Heinrich cold events H1 to H4 (16.8, 24, 31, and 38 ka, respectively) as recorded in North Atlantic deep sea sediment cores [*Hemming*, 2004, and reference therein]. The occurrence of the observed rapid episodes of higher physical erosion in our record may support a connection between weathering regime and the South Asian monsoon intensity in the Irrawaddy catchment and northern hemisphere millennial variability, as previously suggested for other regions [e.g., *Kudrass et al.*, 2001]. A minimum in smectite/(illite + chlorite) and higher ^{87}Sr/^{86}Sr ratios document an episode of high physical erosion ~52 ka which may correspond to Heinrich event H5a recorded in the Labrador Sea, the North Atlantic, and off northeast Brazil [*Rashid et al.*, 2003; *Jaeschke et al.*, 2007]. The

other weathering proxy records obtained from the Bay of Bengal (Chemical Index of Alteration results in Figure 7) [*Colin et al*., 1998] also indicate a weaker South Asian monsoon associated with Heinrich intervals. The record of the monsoon-forced biological productivity in the northwestern Arabian Sea suggest a weak South Asian summer monsoon during the Heinrich events of the North Atlantic Ocean [*Schulz et al*., 1998; *Schulte and Müller*, 2001; *Deplazes et al*., 2014]. Furthermore, a weak Asian summer monsoon during the last glacial Heinrich intervals is also suggested by the $\delta^{18}O$ of speleothems from Indian (Timta), and Chinese (Songjia, Dongge and Hulu) caves [*Wang et al*., 2001; *Pausata et al*., 2011, and references therein].

The overall pattern of the clay mineral assemblages and Sr isotope ratio records agree well with other chemical weathering records from the region (e.g., CIA; Figure 7) [*Colin et al*., 1998] but the timing of the weaker monsoon events during the glacial differs from that of the sea surface temperature records obtained from the northern Andaman Sea [*Marzin et al*., 2013], the $\delta^{18}O$ from the Hulu cave speleothem in China [*Wang et al*., 2001], and aeolian dust records (Zr/Al) from the Arabian Sea [*Deplazes et al*., 2014]. Although the resolution of our records makes this hard to interpret, there appears to be a delay in the weathering response to weaker monsoon intervals. This time lag of a thousand years or more possibly results from the time needed to transport clays from the location of physical erosion during a period of drier climate.

In summary, the proxy records of physical erosion and chemical weathering indicate that the intensity of the South Asian summer monsoon over the Irrawaddy catchment may have been linked to the climatic patterns of the North Atlantic Ocean. However, an unambiguous relationship between South Asian monsoon-related changes in weathering intensity and northern hemisphere millennial scale climatic variability cannot be evaluated here due to the insufficient of the precision of the age model and low sample resolution.

5. Conclusions

The radiogenic Nd and Pb isotope compositions of the detrital clay-size fraction of the NGHP Site 17 in the Andaman Sea show that over the past 60 kyr detrital clays were mainly sourced from the Irrawaddy catchment including the Indo-Burman Ranges with a minor contribution from nearby local sources (Andaman Islands, Barren Island). This suggests that the monsoon over the Irrawaddy catchment was spatially stable during the last glacial and deglaciation. The clay mineral assemblages and Sr isotope compositions of the clays mainly reflect changes in physical erosion and chemical weathering. High smectite contents and smectite/(illite + chlorite) ratios and relatively low radiogenic $^{87}Sr/^{86}Sr$ ratios of the clays document that a stronger monsoon intensity prevailing during the early Holocene compared to the last glacial period. During the glacial distinct minima in smectite/(illite + chlorite) ratios and peak radiogenic Sr isotope signatures mark short periods of weaker South Asian monsoon intensity and drier conditions in the source areas of the sediments. These dry events in the Irrawaddy catchment were possibly linked to the northern hemisphere Heinrich cold events, although this cannot be unambiguously proven based on the currently available data and the limitations of the age model.

Acknowledgments
Part of this work was funded by German Science Foundation (DFG), grant HA5751/3-1. Jutta Heinze is thanked for her help in the laboratory and XRD measurements. Nabil Khélifi is highly thanked for constructive discussions and suggestions during the preparation of the paper. All data used in the figures are either presented in the tables (our data) or their source publications have been referenced.

References

Abouchami, W., S. J. G. Galer, and A. Koschinsky (1999), Pb and Nd isotopes in NE Atlantic Fe-Mn crusts: Proxies for trace metal paleosources and paleocean circulation, *Geochim. Cosmochim. Acta*, *63*, 1489–1505.

Ahmad, S. M., G. Anil Babu, V. M. Padmakumari, A. M. Dayal, B. S. Sukhija, and P. Nagabhushanam (2005), Sr, Nd isotopic evidence of terrigenous flux variations in the Bay of Bengal: Implications of monsoons during the last ~34,000 years, *Geophys. Res. Lett.*, *32*, L22711, doi: 10.1029/2005GL024519.

Albarède, F., P. Telouk, J. Blichert-Toft, M. Boyet, A. Agranier, and B. Nelson (2004), Precise and accurate isotopic measurements using multiple-collector ICPMS, *Geochim. Cosmochim. Acta*, *68*, 2725–2744.

Allen, R., et al. (2008a), New constraints on the sedimentation and uplift history of the Andaman-Nicobar accretionary prism, South Andaman Island, *Geol. Soc. Am. Spec. Pap.*, *436*, 223–255.

Allen, R., Y. Najman, A. Carter, D. Barfod, M. J. Bickle, H. J. Chapman, E. Garzanti, G. Vezzoli, S. Ando, and R. R. Parrish (2008b), Provenance of the Tertiary sedimentary rocks of the Indo-Burman Ranges, Burma (Myanmar): Burman arc or Himalayan-derived?, *J. Geol. Soc.*, *165*, 1045–1057.

An, Z. (2000), The history and variability of the East Asian paleomonsoon climate, *Quat. Sci. Rev.*, *19*(1–5), 171–187.

Awasthi, N., J. S. Ray, A. K. Singh, S. T. Band, and V. K. Rai (2014), Provenance of the Late Quaternary sediments in the Andaman Sea: Implications for monsoon variability and ocean circulation, *Geochem. Geophys. Geosyst.*, *15*, 3890–3906, doi:10.1002/2014GC005462.

Barrat, J. A., F. Keller, J. Amossé, R. N. Taylor, R. W. Nesbitt, and T. Hirata (1996), Determination of rare earth elements in sixteen silicate reference samples by ICP-MS after Tm addition and ion exchange separation, *Geostand. Newsl.*, *20*, 133–139.

Bayon, G., C. R. German, R. M. Boella, J. A. Milton, R. N. Taylor, and R. W. Nesbitt (2002), An improved method for extracting marine sediment fractions and its application to Sr and Nd isotopic analysis, *Chem. Geol.*, *187*, 179–199.
Bender, F. K. (1983), *Geology of Burma*, 322 pp., Gebruder Borntraeger Verlagsbuchhandlung, Science Publ., Berlin.
Blum, J. D., Y. Erel, and K. Brown (1993), $^{87}Sr/^{86}Sr$ ratios of Sierra Nevada stream waters: Implications for relative mineral weathering rates, *Geochim. Cosmochim. Acta*, *57*(21–22), 5019–5025.
Bunsomboonsakul, S., Z. F. Liu, P. Sompongchaiyakul, A. Snidvongs, and S. Karstel (2010), Clay mineralogical records in sediments along the Shelf Break of the eastern Andaman Sea, *Eos Trans. AGU*, *90*(52), Fall Meet. Suppl., Abstract PP31C-2057.
Caley, T., B. Malaizé, S. Zaragosi, L. Rossignol, J. Bourget, F. Eynaud, P. Martinez, J. Giraudeau, K. Charlier, and N. Ellouz-Zimmermann (2011), New Arabian Sea records help decipher orbital timing of Indo-Asian monsoon, *Earth Planet. Sci. Lett.*, *308*(3–4), 433–444.
Chamley, H. (1989), *Clay Sedimentology*, 656 pp., Springer, N. Y.
Clemens, S., W. Prell, D. Murray, G. Shimmield, and G. Weedon (1991), Forcing mechanisms of the Indian Ocean monsoon, *Nature*, *353*, 720–725.
Clift, P. D., L. Giosan, J. Blusztajn, I. H. Campbell, C. Allen, M. Pringle, A. R. Tabrez, M. Danish, M. Rabbani, and A. Alizai (2008), Holocene erosion of the Lesser Himalaya triggered by intensified summer monsoon, *Geology*, *36*(1), 79–82.
Cohen, A. S., R. K. O'Nions, R. Siegenthaler, and W. L. Griffin (1988), Chronology of the pressure-temperature history recorded by a granulite terrain, *Contrib. Mineral. Petrol.*, *98*, 303–311.
Colin, C., C. Kissel, D. Blamart, and L. Turpin (1998), Magnetic properties of sediments in the Bay of Bengal and the Andaman Sea: Impact of rapid North Atlantic Ocean climatic events on the strength of the Indian monsoon, *Earth Planet. Sci. Lett.*, *160*, 623–635.
Colin, C., L. Turpin, J. Bertaux, A. Desprairies, and C. Kissel (1999), Erosional history of the Himalayan and Burman ranges during the last two glacial-interglacial cycles, *Earth Planet. Sci. Lett.*, *171*(4), 647–660.
Colin, C., L. Turpin, D. Blamart, N. Frank, C. Kissel, and S. Duchamp (2006), Evolution of weathering patterns in the Indo-Burman Ranges over the last 280 kyr: Effects of sediment provenance on $^{87}Sr/^{86}Sr$ ratios tracer, *Geochem. Geophys. Geosyst.*, *7*, Q03007, doi:10.1029/2005GC000962.
Collett, T. S., M. Riedel, J. R. Cochran, R. Boswell, J. Presley, P. Kumar, A. Sathe, M. Lall, V. Sibal, and the NGHP Expedition 01 Scientist (2008), National gas hydrate program Expedition 01, initial report, Dir. Gen. of Hydrocarbon, New Delhi, India.
Depaolo, D. J. (1980), Sources of continental crust: Neodymium isotope evidence from the Sierra Nevada and peninsular ranges, *Science*, *209*, 684–687.
DePaolo, D. J. (1981), Neodymium isotopes in the Colorado Front Range and crust-mantle evolution in the Proterozoic, *Nature*, *291*, 193–196.
Deplazes, G., A. Lückge, J.-B. W. Stuut, J. Pätzold, H. Kuhlmann, D. Husson, M. Fant, and G. H. Haug (2014), Weakening and strengthening of the Indian monsoon during Heinrich events and Dansgaard-Oeschger oscillations, *Paleoceanography*, *29*, 99–114, doi:10.1002/2013PA002509.
Dia, A., B. Dupré, and C. J. Allègre (1992), Nd isotopes in Indian Ocean sediments used as a tracer of supply to the ocean and circulation paths, *Mar. Geol.*, *103*, 349–359.
Dickin, A. P. (2005), *Radiogenic Isotope Geology*, 2nd ed., 512 pp., Cambridge Univ. Press, Cambridge, U. K.
Egli, M., A. Mirabella, and P. Fitze (2001), Clay mineral formation in soils of two different chronosequences in the Swiss Alps, *Geoderma*, *104*, 145–175.
Ehlert, C., M. Frank, B. A. Haley, U. Böniger, P. DeDeckker, and F. X. Gingele (2011), Current transport versus continental inputs in the eastern Indian Ocean: Radiogenic isotope signatures of clay size sediments, *Geochem. Geophys. Geosyst.*, *12*, Q06017, doi:10.1029/2011GC003544.
Fagel, N., C. Innocent, C. Gariepy, and C. Hillaire-Marcel (2002), Sources of Labrador Sea sediments since the last glacial maximum inferred from Nd-Pb isotopes, *Geochim. Cosmochim. Acta*, *66*, 2569–2581.
Fagel, N., C. Hillaire-Marcel, M. Humblet, R. Brasseur, D. Weis, and R. Stevenson (2004), Nd and Pb isotope signatures of the clay-size fraction of Labrador Sea sediments during the Holocene: Implications for the inception of the modern deep circulation pattern, *Paleoceanography*, *19*, PA3002, doi:10.1029/2003PA000993.
Fagel, N., C. Not, J. Gueibe, N. Mattielli, and E. Bazhenova (2014), Late Quaternary evolution of sediment provenances in the Central Arctic Ocean: Mineral assemblage, trace element composition and Nd and Pb isotope fingerprints of detrital fraction from the Northern Mendeleev Ridge, *Quat. Sci. Rev.*, *92*, 140–154.
Flores, J. A., A. E. Mejia-Molina, M. C. Alvarez, F. J. Sierro, S. D. Singh, S. Mahanti, and L. Giosan (2014), Sedimentation rates from calcareous nannofossil and planktonic foraminifera biostratigraphy in the Andaman Sea, northern Bay of Bengal, and Eastern Arabian Sea, *J. Mar. Petrol. Geol.*, *58*(Part A), 425–437.
Galer, S. J. G., and R. K. O'nions (1989), Chemical and isotopic studies of ultramafic inclusions from the San Carlos Volcanic Field, Arizona: A bearing on their petrogenesis, *J. Petrol.*, *30*, 1033–1064.
Garçon, M., C. Chauvel, C. France-Lanord, M. Limonta, and E. Garzanti (2013), Removing the "heavy mineral effect" to obtain a new Pb isotopic value for the upper crust, *Geochem. Geophys. Geosyst.*, *14*, 3324–3333, doi:10.1002/ggge.20219.
Garçon, M., C. Chauvel, C. France-Lanord, M. Limonta, and E. Garzanti (2014), Which minerals control the Nd-Hf-Sr-Pb isotopic compositions of river sediments?, *Chem. Geol.*, *364*, 42–55.
Garzanti, E., M. Limonta, A. Resentini, P. C. Bandopadhyay, Y. Najman, S. Andò, and G. Vezzoli (2013), Sediment recycling at convergent plate margins (Indo-Burman Ranges and Andaman-Nicobar Ridge), *Earth Sci. Rev.*, *123*, 113–132.
Gingele, F. X., and P. DeDeckker (2004), Fingerprinting Australia's rivers with clay minerals and the application for the marine record of climate change, *Aust. J. Earth Sci.*, *51*, 339–348.
Gingele, F. X., F. Schmieder, T. von Dobeneck, R. Petschick, and C. Rühlemann (1999), Terrigenous flux in the Rio Grande rise area during the past 1500 ka: Evidence of deepwater advection or rapid response to continental rainfall patterns?, *Paleoceanography*, *14*, 84–95.
Goldstein, S. J., and S. B. Jacobsen (1988), Nd and Sr isotopic systematics of river water suspended material: Implications for crustal evolution, *Earth Planet. Sci. Lett.*, *87*, 249–265.
Griffin, J. J., H. Windom, and E. D. Goldberg (1968), The distribution of clay minerals in the World Ocean, *Deep Sea Res. Oceanogr. Abstr.*, *15*, 433–459.
Hemming, S. R. (2004), Heinrich events: Massive late Pleistocene detritus layers of the North Atlantic and their global climate imprint, *Rev. Geophys.*, *42*, RG1005, doi:10.1029/2003RG000128.
Hemming, S. R., S. McLennan, and G. Hanson (1995), Geochemical and Nd/Pb isotopic evidence for the provenance of the Early Proterozoic Virginia Formation, Minnesota. Implications for the tectonic setting of the Animikie Basin, *J. Geol.*, *103*, 147–168.
Horwitz, E. P., R. Chiarizia, and M. L. Dietz (1992), A novel strontium-selective extraction chromatographic resin*, *Solvent Extract. Ion Exch.*, *10*, 313–336.

Hu, B., G. Li, J. Li, J. Bi, J. Zhao, and R. Bu (2012), Provenance and climate change inferred from Sr-Nd-Pb isotopes of late Quaternary sediments in the Huanghe (Yellow River) Delta, China, *Quat. Res.*, *78*, 561–571.

Huang, C.-Y., P.-M. Liew, M. Zhao, T.-Z. Chang, C.-M. Kuo, M.-T. Chen, C.-H. Want, and L.-F. Zheng (1997), Deep sea and lake records of the Southeast Asian paleomonsoons for the last 25 thousands years, *Earth Planet. Sci. Lett.*, *146*, 59–72.

IOC, IHO, and BODC (2003), *Centenary Edition of the GEBCO Digital Atlas, Published on CD-ROM on Behalf of the Intergovernmental Oceanographic Commission and the Internatioanl Hydrographic Organization as Part of the General Bathymetric Chart of the Oceans*, Br. Oceanogr. Data Cent., Liverpool, U. K.

Jacobsen, S. B., and G. J. Wasserburg (1980), Sm-Nd isotopic evolution of chondrites, *Earth Planet. Sci. Lett.*, *50*, 139–155.

Jaeschke, A., C. Rühlemann, H. Arz, G. Heil, and G. Lohmann (2007), Coupling of millennial-scale changes in sea surface temperature and precipitation off northeastern Brazil with high-latitude climate shifts during the last glacial period, *Paleoceanography*, *22*, PA4206, doi: 10.1029/2006PA001391.

Johnson, J. E., S. C. Phillips, M. E. Torres, E. Pinero, K. K Rose, and L. Giosan (2014), Influence of total organic carbon deposition on the inventory of gas hydrate in the Indian continental margins, *J. Mar. Petrol. Geol.*, *58*(Part A), 406–424.

Krumm, S. (2006), *SediCalc (Free Geological Software), GeoZentrum Nordbayern*, Univ. Erlangen-Nürnberg. [Available at http://www.geol.uni-erlangen.de/sedicalc.]

Kudrass, H., A. Hofmann, H. Doose, K. Emeis, and H. Erlenkeuser (2001), Modulation and amplification of climatic changes in the Northern Hemisphere by the Indian summer monsoon during the past 80 ky, *Geology*, *29*(1), 63–66.

Kumar, O. S. R. U. B., C. Naidu, S. Rao, and B. R. Srinivasa Rao (2004), Prediction of southern Indian winter monsoon rainfall from September local upper-air temperatures, *Meteorol. Appl.*, *11*(3), 189–199.

Kurian, S., B. N. Nath, V. Ramaswamy, D. Naman, T. Gnaneshwar Rao, K. A. Kamesh Raju, K. Selvaraj, and C. T. A. Chen (2008), Possible detrital, diagenetic and hydrothermal sources for Holocene sediments of the Andaman backarc basin, *Mar. Geol.*, *247*(3–4), 178–193.

Lau, K. M., and S. Yang (1997), Climatolog and interannual variability of the southeast Asian summer monsoon, *Adv. Atmos. Sci.*, *14*(2), 141–162.

Le Fèvre, B., and C. Pin (2005), A straightforward separation scheme for concomitant Lu-Hf and Sm-Nd isotope ratio and isotope dilution analysis, *Anal. Chim. Acta*, *543*, 209–221.

Licht, A., C. France-Lanord, L. Reisberg, C. Fontaine, A. N. Soe, and J. J. Jaeger (2013), A paleo Tibet-Myanmar connection? Reconstructing the Late Eocene drainage system of central Myanmar using a multi-proxy approach, *J. Geol. Soc. London*, *170*, 929–939.

Lisiecki, L. E., and M. E. Raymo (2005), A Pliocene-Pleistocene stack of 57 globally distributed benthic δ^{18}O records, *Paleoceanography*, *20*, PA1003, doi:10.1029/2004PA001071.

Liu, Z., C. Colin, W. Huang, K. P. Le, S. Tong, Z. Chen, and A. Trentesaux (2007), Climatic and tectonic controls on weathering in south China and Indochina Peninsula: Clay mineralogical and geochemical investigations from the Pearl, Red, and Mekong drainage basins, *Geochem. Geophys. Geosyst.*, *8*, Q05005, doi:10.1029/2006GC001490.

Lovett, R. A. (2010), Tree rings map 700 years of Asian monsoons, *Nat. News*. [Available at http://www.nature.com/news/2010/100422/full/news.2010.196.html.]

Lugmair, G. W., and S. J. G. Galer (1992), Age and isotopic relationships among the angrites Lewis Cliff 86010 and Angra dos Reis, *Geochim. Cosmochim. Acta*, *56*, 1673–1694.

Luhr, J. F., and D. Haldar (2006), Barren Island Volcano (NE Indian Ocean): Island-arc high-alumina basalts produced by troctolite contamination, *J. Volcanol. Geotherm. Res.*, *149*, 177–212.

Mark, D. F., M. Petraglia, V. C. Smith, L. E. Morgan, D. N. Barfod, B. S. Ellis, N. J. Pearce, J. N. Pal, and R. Korisettar (2014), A high-precision ^{40}Ar/^{39}Ar age for the Young Toba Tuff and dating of ultra-distal tephra: Forcing of Quaternary climate and implications for hominin occupation of India, *Quat. Geochronol.*, *21*, 90–103.

Marzin, C., N. Kallel, M. Kageyama, J. C. Duplessy, and P. Braconnot (2013), Glacial fluctuations of the Indian monsoon and their relationship with North Atlantic climate: New data and modelling experiments, *Clim. Past*, *9*, 2135–2151.

McDaniel, D., S. Hemming, S. McLennan, and G. Hanson (1994), Resetting of neodymium isotopes and redistribution of REEs during sedimentary processes: The Early Proterozoic Chelmsford Formation, Sudbury Basin, Ontario, Canada, *Geochim. Cosmochim. Acta*, *58*(2), 931–941.

McLennan, S. M., and S. Hemming (1992), Samarium/neodymium elemental and isotopic systematics in sedimentary rocks, *Geochim. Cosmochim. Acta*, *56*, 887–898.

McLennan, S. M., S. Hemming, D. K. McDaniel, and G. N. Hanson (1993), Geochemical approaches to sedimentation, provenance, and tectonics, *Geol. Soc. Am. Spec. Pap.*, *284*, 21–40.

Meyer, I., G. R. Davies, and J. B. W. Stuut (2011), Grain size control on Sr-Nd isotope provenance studies and impact on paleoclimate reconstructions: An example from deep-sea sediments offshore NW Africa, *Geochem. Geophys. Geosyst.*, *12*, Q03005, doi:10.1029/2010GC003355.

Millot, R., C. J. Allègre, J. Gaillardet, and S. Roy (2004), Lead isotopic systematics of major river sediments: A new estimate of the Pb isotopic composition of the Upper Continental Crust, *Chem. Geol.*, *203*(1), 75–90.

NASA (1999). [Available at http://eoimages.gsfc.nasa.gov/images/imagerecords/53000/53677/S1999364054204_md.jpg.]

Nath, B. N., A. Makishima, J. Noordmann, R. Ranaka, and E. Nakamura (2009), Comprehensive analysis for major, minor and trace element contents and Sr-Nd-Pb-Hf isotope ratios in sediment reference materials, JSd-1 and MAG-1, *Geochem. J.*, *43*, 207–216.

Paillard, D., L. Labeyrie, and P. Yiou (1996), Macintosh program performs time-series analysis, *Eos Trans. AGU*, *77*(39), 379–379.

Pausata, F. S. R., D. S. Battisti, K. H. Nisancioglu, and C. M. Bitz (2011), Chinese stalagmite δ^{18}O controlled by changes in the Indian monsoon during a simulated Heinrich event, *Nat. Geosci.*, *4*, 474–480.

Phillips, S. C., J. E. Johnson, M. B. Underwood, J. Guo, L. Giosan, and K. Rose (2014), Long-timescale variation in bulk and clay mineral composition of Indian continental margin sediments in the Bay of Bengal, Arabian Sea, and Andaman Sea, *Mar. Petrol. Geol.*, *58*, 117–138.

Pokhrel, S., H. S. Chaudhari, S. Saha, A. Dhakate, R. K. Yadav, K. Salunke, S. Mahapatra, and S. Rao (2012), ENSO, IOD and Indian Summer Monsoon in NCEP climate forecast system, *Clim. Dyn.*, *39*(9–10), 2143–2165.

Rashid, H., R. Hesse, and D. J. W. Piper (2003), Evidence for an additional Heinrich event between H5 and H6 in the Labrador Sea, *Paleoceanography*, *18*(4), 1077, doi:10.1029/2003PA000913.

Rashid, H., B. P. Flower, R. Z. Poore, and T. M. Quinn (2007), A ~25 ka Indian Ocean monsoon variability record from the Andaman Sea, *Quat. Sci. Rev.*, *26*, 2586–2597.

Rashid, H., E. England, L. Thompson, and L. Polyak (2011), Late glacial to holocene Indian summer monsoon variability based upon sediment records taken from the Bay of Bengal, *Terr. Atmos. Oceanic Sci.*, *22*, 215.

Rizal, S., et al. (2012), General circulation in the Malacca Strait and Andaman Sea: A numerical model study, *Am. J.. Environ. Sci.*, *8*, 479–488.

Robinson, R. A. J., et al. (2007), The Irrawaddy river sediment flux to the Indian Ocean: The original nineteenth-century data revisited, *J. Geol.*, *115*, 629–640.

Robinson, R. A. J., et al. (2014), Large river and orogens: The evolution of the Yarlung Tsangpo-Irrawaddy system and the eastern Himalayan syntaxis, *Gondwana Res.*, *26*(1), 112–121.

Rose, K., J. E. Johnson, M. Torres, W. Hong, L. Giosan, E. Solomon, M. Kastner, T. Cawthern, P. Long, and H. Schaef (2014), Preferential accumulation of gas hydrate in porous-permeable volcanic ash beds of the Andaman Arc, NGHP-01 site 17A, *J. Mar. Petrol. Geol.*, *58*(Part A), 99–116.

Schulte, S., and P. J. Müller (2001), Variations of sea surface temperature and primary productivity during Heinrich and Dansgaard-Oeschger events in the northeastern Arabian Sea, *Geo Mar. Lett.*, *21*, 168–175.

Schulz, U. H., U. U. von Rad, and U. H. Erlenkeuser (1998), Correlation between Arabian Sea and Greenland climate oscillations of the past 110,000 years, *Nature*, *393*, 54–57.

Smith, V. C., N. J. G. Pearce, N. E. Matthews, J. A. Westgate, M. D. Petraglia, M. Haslam, C. S. Lane, R. Korisettar, and J. N. Pal (2011), Geochemical fingerprinting of the widespread Toba tephra using biotite compositions, *Quat. Int.*, *246*(1–2), 97–104.

Stuiver, M., P. J. Reimer, and R. Reimer (2014), Calib 7.0. [Available at http://calib.qub.ac.uk/calib/.]

Southon, J., M. Kashgarian, M. Fontugne, B. Metivier, and W. W.-S. Yim (2002), Marine reservoir corrections for the Indian ocean and southeast Asia, *Radiocarbon*, *44*, 167–180.

Stacey, J. T., and J. Kramers (1975), Approximation of terrestrial lead isotope evolution by a two-stage model, *Earth Planet. Sci. Lett.*, *26*(2), 207–221.

Steiger, R. H., and E. Jäger (1977), Subcommission on geochronology: Convention on the use of decay constants in geo- and cosmochronology, *Earth Planet. Sci. Lett.*, *36*, 359–362.

Stumpf, R., M. Frank, J. Schönfeld, and B. A. Haley (2011), Climatically driven changes in sediment supply on the SW Iberian shelf since the Last Glacial Maximum, *Earth Planet. Sci. Lett.*, *312*(1), 80–90.

Tanaka, T., et al. (2000), JNdi-1: A neodymium isotopic reference in consistency with LaJolla neodymium, *Chem. Geol.*, *168*, 279–281.

Taylor, A., and J. D. Blum (1995), Relation between soil age and silicate weathering rates determined from the chemical evolution of a glacial chronosequence, *Geology*, *23*, 979–982.

Taylor, S. R., and S. M. McLennan (1985), *Its Composition and Evolution: An Examination of the Geochemical Record Preserved in Sedimentary Rocks*, 312 pp., Blackwell Sci., Oxford, U. K.

Thiry, M. (2000), Palaeoclimatic interpretation of clay minerals in marine deposits: An outlook from the continental origin, *Earth Sci. Rev.*, *49*, 201–221.

Tütken, T., A. Eisenhauer, B. Wiegand, and B. T. Hansen (2002), Glacial-interglacial cycles in Sr and Nd isotopic composition of Arctic marine sediments triggered by the Svalbard/Barents Sea ice sheet, *Mar. Geol.*, *182*, 351–372.

van Kreveld, S., M. Sarnthein, H. Erlenkeuser, P. Grootes, S. Jung, M. J. Nadeau, U. Pflaumann, and A. Voelker (2000), Potential links between surging ice sheets, circulation changes, and the Dansgaard-Oeschger Cycles in the Irminger Sea, 60–18 Kyr, *Paleoceanography*, *15*, 425–442.

von Blanckenburg, F., and T. F. Nägler (2001), Weathering versus circulation-controlled changes in radiogenic isotope tracer composition of the Labrador Sea and North Atlantic Deep Water, *Paleoceanography*, *16*, 424–434.

Wang, Y. J., H. Cheng, R. L. Edwards, Z. S. An, J. Y. Wu, C.-C. Shen, and J. A. Dorale (2001), A high-resolution absolute-dated late Pleistocene monsoon record from Hulu Cave, China, *Science*, *294*, 2345–2348.

Xie, S. P., H. Xu, N. H. Saji, Y. Wang, and T. Liu (2006), Role of narrow mountains in large-scale organization of Asian monsoon convection, *J. Clim.*, *19*(14), 3420–3429.

Erratum

In the originally published version of this article, an incorrect paper was listed for *Phillips et al.* (2014) in the reference list. The following has since been corrected and this version may be considered the authoritative version of record.

Phillips, S. C., J. E. Johnson, L. Giosan, and K. Rose (2014), Monsoon-influenced variation in productivity and lithogenic sediment flux since 110 ka in the offshore Mahanadi Basin, northern Bay of Bengal, *Mar. Petrol. Geol.*, 58(Part A), 502–525, has been changed to Phillips, S.C., Johnson, J.E., Underwood, M.B., Guo, J., Giosan, L., and Rose, K., 2014. Long-timescale variation in bulk and clay mineral composition of Indian continental margin sediments in the Bay of Bengal, Arabian Sea, and Andaman Sea, *Mar. Petrol. Geol.*, 58, 117–138.